Insights on Carbon Nanotubes and Fullerenes in Molten Alkali Carbonates

Alberto Gutiérrez,[a,b] Sebastiano Garroni,[c] Stamatios Souentie,[d] Santiago Cuesta-López,[b] Iakovos Yakoumis,*[d] and Santiago Aparicio,*[a,b]

[a] Department of Chemistry, University of Burgos, 09001 Burgos, Spain

[b] International Research Centre in Critical Raw Materials-ICCRAM, University of Burgos, 09001 Burgos, Spain

[c] Department of Chemistry and Pharmacy, Università degli Studi di Sassari, 07100 Sassari, Italy

[d] MONOLITHOS Catalysts & Recycling Ltd, 11476 Athens, Greece

*Corresponding authors: yakoumis@monolithos-catalysts.gr (I. Y.) and sapar@ubu.es (S. A.)

ABSTRACT: The properties of single wall carbon nanotubes and carbon fullerenes in molten alkali carbonates were studied as a function of the considered nanomaterial and the ions into the molten salt using classical molecular dynamics simulations. The adsorption and confinement in carbon nanotubes is developed by efficient adsorption of carbonate ions in inner and outer walls of the nanotubes whereas alkali cations do not show remarkable interaction with the nanomaterial. Analogous solvation mechanisms are inferred for carbon fullerenes with large disruption of the liquid structuring of molten alkali carbonate at high fullerene concentrations. The solvation ability of the studied lithium-sodium-potassium carbonate eutectic mixture for both types of nanomaterials are suitable for considering this fluid in the development of composite materials for advanced technological applications.

1
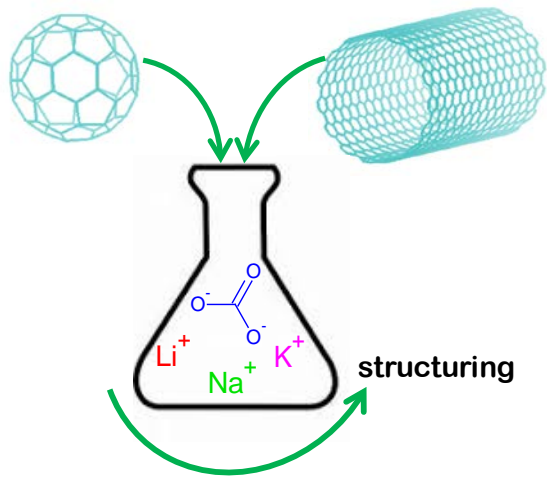
Table of Contents Graphic

Introduction

Molten salts (MSs) have received great attention in industry and academia for many technological applications, especially for high-temperature thermal energy storage[1] and heat transfer applications.[2] MSs are considered as engineering fluids,[3] with a great potential in renewable energy applications, such as concentrated solar power plants (CSPs),[4] considering energy storage and transformation processes.[5,6,7] The most relevant thermophysical properties of MSs are largely suitable for energy-related technologies,[8] in particular when considering thermal and transport properties. Molten alkali carbonates (MACs) exhibit high thermal stability at high temperatures,[9,10,11] which is pivotal for high temperature applications. They also show very low vapor pressure, [12] wide liquid range, low viscosity[13] (which decreases pumping costs) and large thermal conductivity. [14,15] Likewise, the low cost of MSs and their reduced environmental impact with suitable biodegradability lead to the consideration of sustainable fluids.[16] Therefore, although some researches have showed some problems on the application of MACs for thermal energy storage, which may affect the stability of MACs – based systems,[17] this technology can be considered as very promising materials availability and the possibility of tuning their properties by additives introduction, e.g. addition of nanoparticles, to improve their performance [18,19].

Molten alkali carbonates (MACs) have also been used as electrolytes in fuel cell applications.[20,21] The molten carbonate fuel cell (MCFC) technology offers strong potential for both power generation and power-chemicals cogeneration in an environmentally friendly way.[22,23] Likewise, MACs have been proposed for gas separation operations, in particular for CO_2 capture and valorisation,[24] which is of great relevance for CO_2 abatement, both using MCFCs[25,26] and absorption on the liquid phase.[27,28] Moreover, MACs – based membranes for gas (CO_2) separation applications have been reported considering several supports.[29,30,31] In particular, MACs on 2D materials such as graphene have showed remarkable and useful properties.[32]

The introduction of particular nanoparticle additives to MSs, has been studied to improve MSs properties, such as to increase the specific heat capacity and other thermal properties.[33,34] Nanomaterials based on embedding carbon nanotubes in a MS

have been proposed for thermal energy storage purposes, showing a remarkable increase in specific heat capacity.[35] Likewise, it may be expected that the addition of other types of carbon-based nanoparticles such as fullerenes may change remarkably the physicochemical properties of MSs. The modifications on the thermal properties of MSs by the addition of carbon nanotubes and/or fullerenes should be due to induced molecular rearrangements of liquid phase structures by the ordering effect produced by the presence of the additives. Studies on the liquid structuring of MSs + carbon nanotubes / fullerenes are absent in the literature. Nevertheless, available studies on related systems formed by low temperature molten salts (i.e. ionic liquids) + carbon nanotubes / fullerenes have showed a large structuring effect induced by the presence of these additives.[36] This is pronounced in the case of carbon nanotubes due to the possibility of ions confinement inside the nanotubes leading to highly structured materials.[37] Therefore, additional studies are required to understand the molecular level (nanoscopic) features of MSs + carbon nanotubes / fullerenes systems, and thus advancing in these mixed materials for energy related applications. For this purpose, mixtures of MACs, as one of the most relevant types of MSs, and single wall carbon nanotubes (SWNTs), or carbon fullerenes (C_{60}), were studied using a theoretical approach based on classical molecular dynamics (MD) simulations to infer the main nanoscopic features of the studied systems. The theoretical study will be concentrated on the features of relevant interfacial regions, since they are essential for the performance of the composite system,[38] considering that intermolecular forces at the interfaces will have a large effect on the macroscopic properties of the mixed material(s). In the case of SWNTs, the properties of confined MACs inside the SWNTs are also studied. The selected MACs were pure Li_2CO_3 (*m.p.* = 996.15 K), pure Na_2CO_3 (*m.p.* = 1124.15 K), pure K_2CO_3 (*m.p.* = 1164.15 K) and the eutectic mixture $Li_{0.87}Na_{0.63}K_{0.50}CO_3$ (i.e. an eutectic mixture composed of 43.5 % Li_2CO_3 + 31.5 % Na_2CO_2 + 25 % K_2CO_3, *m.p.* = 673 K)[39] for analyzing the behavior high and low melting point MACs as well as the effect of the additives in a complex eutectic mixture. The reported results are analysed in terms of structuring at interfaces, ions adsorption and changes in MACs properties upon formation of composite systems. Likewise, dynamic properties of molecules at interfacial regions were studied together with the strength

of intermolecular interactions determining the main characteristics of SWNT's/C_{60} – MACs nanocomposites.

Methods

MDynaMix v.5.2 molecular modelling package[40] was used for all the MD simulations. The force field parameterizations for MACs ions are reported in Table S1 (Supporting Information) and were obtained from Roest et al.[38] SWNTs and C_{60} fullerene were modelled as a rigid entities, i.e. frozen along the simulations. SWNTs studied were hydrogen terminated entities with force field parameters as well as those for C_{60} obtained from a previous work,[41] and reported in Table S1 (Supporting Information). The MACs (Li_2CO_3 or Na_2CO_3 or K_2CO_3 or $Li_{0.87}Na_{0.63}K_{0.50}CO_3$ eutectic mixture) + SWNT / C_{60} systems used for molecular dynamics simulations were reported in Table S2 (Supporting Information). Simulations were carried out using periodic boundary conditions were applied in the three space directions. Initial simulation boxes were built using Packmol program[42] placing SWNTs or C_{60} fullerene in the center of cubic simulation boxes being surrounded by the corresponding MAC. The studied SWNTs were: *i*) an armchair SWNT with chirality (6,6), 3.4 nm long and 0.9 nm diameter (360 carbon atoms and 24 terminal hydrogen atoms), *ii*) an armchair SWNT with chirality (15,15), 3.4 nm long and 2 nm dimeter (900 carbon atoms and 60 terminal hydrogen atoms) and *iii*) an armchair SWNT with chirality (25,25), 3.4 nm long and 3.4 nm dimeter (1500 carbon atoms and 100 terminal hydrogen atoms). The size of the simulation boxes was $68 \times 68 \times 68$ Å^3, which when comparing with SWNTs length leads to boxes two times larger than the SWNTs, thus discarding interactions with neighbor simulation cells. Regarding simulations involving fullerene, two types of simulations were carried out. First, a single C_{60} fullerene molecule was placed at the center of simulation boxes and surrounded by the corresponding MAC (to analyze the solvation of fullerene). Second, a system with 6 C_{60} fullerenes randomly distributed in the simulation cell were surrounded by the MACs.

All MD simulation were carried out according to a two-step procedure: i) equilibration in the NVT ensemble (assured by the constancy of total potential energy) followed by ii) production runs in the NPT ensemble (10 ns long). Simulations at 1023, 1153, 1193 and 673K were performed for systems containing Li_2CO_3, Na_2CO_3, K_2CO_3

and $Li_{0.87}Na_{0.63}K_{0.50}CO_3$, respectively, i.e., molten salts were present in all simulation cases. Regarding possible doubts on the stability of carbon nanotubes and fullerenes at the temperatures used in the simulations, studies in the literature have showed that SWNTs are stable at temperatures up to 3073K in vacuum, while no remarkable degradation is inferred for applications up to 1023K in air.[43] In the case of fullerene, Eletskii et al.[44] and Millican et al.[45] state that C_{60} molecule is stable in an inert (Ar) atmosphere at temperatures up to 1200K. In other studies[46,47] it is ascertained that C_{60} retains its thermal stability up to 1700K.

The Nose–Hoover method was used for the control of temperature and pressure. Ewald method was applied for handling Coulombic interactions (15 Å cut-off radius). Tuckerman–Berne double time step algorithm[48] (1 and 0.1 fs for long and short time steps) was considered for solving equations of motion. Lorentz-Berthelot mixing rules allowed the calculation of cross Lennard-Jones terms. A cutoff of 15 Å was considered for Lennard-Jones interactions.

Results and discussion

Four different MACs (Li_2CO_3 or Na_2CO_3 or K_2CO_3 or $Li_{0.87}Na_{0.63}K_{0.50}CO_3$ eutectic mixture) were considered in this work and their behaviour with systems containing carbon SWNTs and C60 fullerene were studied using MD simulations, with the main nanoscopic properties being discussed in the following sections.

MACs + carbon SWNTs

Three different types of SWNTs, (6,6), (15,15) and (25,25), were considered in this work regarding the various MACs systems. MACs + SWNTs show two main different features which will be analysed in separate: *i*) SWNTs solvation (i.e. MACs behaviour in the external shell of SWNTs and possible development of external adsorbed layers) and *ii*) MACs confinement inside SWNTs (i.e. behaviour of MACs under cylindrical pore confinement). Firstly, the behaviour of Li_2CO_3 MAC will be analysed and then the remaining salts will be considered to infer the effect of the involved type of cation on systems' properties. The solvation of SWNTs should be characterized by a rearrangement of MACs ions in the region around the external shell of SWNTs, and thus leading to ions–SWNTs interactions, which may be quantified

through the intermolecular interaction energy (E_{inter}, defined as the sum of Lennard-Jones and Coulombic contributions), Figure 1. Data for E_{inter} in Li_2CO_3 + SWNTs reported in Figure 1 are reported for the different ion–SWNT contributions, showing that E_{inter} for Li–SWNTs are positive for the three studied SWNTs (increasing with increasing SWNT diameter, Figure 1a), negative for CO_3^{2-} (also increasing in absolute value with increasing SWNT size, Figure 1d) and the balance for all the ions being negative (Figure 1e), thus confirming that the adsorption of Li_2CO_3 on SWNTs external surface is energetically favoured. The almost linear increase of E_{inter} with SWNT diameter, i.e. with number of C atoms in the SWNT, shows increasing adsorption efficiency by ion – C contacts mainly in the first adsorbed layer. The development of adsorbed layers around the SWNTs is confirmed in results reported in Figure 2. Up to three well defined solvation shells are inferred for CO_3^{2-} anions around all the considered SWNTs. The first shell appears at 4.4 Å of the SWNTs surface and the consecutive solvation shells are separated 3.5 Å; this structuring is maintained independently of the SWNT diameter. The CO_3^{2-} densification around SWNTs is confirmed by number density profiles reported in Figure 2. Nevertheless, the widening of the number density peaks on going from the first solvation shell toward further shell shows more disrupted solvation layers when the distance to the SWNTs decreases. Regarding the arrangement of Li^+ cations, number density profiles reported in Figure 2 show poorly defined adsorption layers, although cation density peaks are inferred, especially for SWNT(25,25), they are wider and less intense than those for CO_3^{2-}, showing poor adsorption ability, in agreement with interaction energies reported in Figure 1. Likewise, number density peaks for Li^+ cations are placed between those corresponding to CO_3^{2-}, e.g. the first density peak for Li^+ is placed 1.2 Å above the first CO_3^{2-} peak. Therefore, the structure of solvation shells around SWNTs is formed by alternating anion-cation layers, although cation layers are poorly defined, thus CO_3^{2-} guide the structuring around carbon nanotubes with cation layers developed for maintaining anion-cation interactions above the nanotubes. Additional features of ions structuring on solvation shells around the SWNTs are inferred in Figure 3, in the case of CO_3^{2-} for large SWNTs (in the case of the studied SWNTs only for SWNT(25,25)) anions adopt a configuration on the first solvation shells forming well defined rows, i.e. anions are arranged in concentric circumferences for the first solvation shell, as confirmed by

the number density profiles in Figure 3d. In the case of Li$^+$ cation this arrangement is absent, and cations are spread over the whole nanotube above the first anion adsorbed layer. Likewise, this orientation is largely dependent on the available adsorption surface, and results in Figures 3a to 3c show that it is absent in small SWNT(6,6), it starts to form in intermediate SWNT(15,15) and kit is fully developed in SWNT(25,25). Additionally, results in Figure 3d show the densification of CO_3^{2-} close to the enter of SWNTs, increasing with increasing SWNT size, and in minor extension for Li$^+$ cations.

The results in Figures 2 and 3 show large densification of CO_3^{2-} on top of SWNTs, density profiles in Figure 4 show the orientation of these anions when adsorbed on the nanotubes surface. The results show that CO_3^{2-} anions are deformed by the presence of SWNTs surface, the planarity of CO_3^{2-} is disrupted leading to a configurations with O atoms placed all above the C atom for all the adsorbed layers although with larger deformations for layers closer to the SWNTs surface (although up to the third adsorbed layers CO_3^{2-} are non-planar ions). The orientations inferred in Figure 4 show alternating configurations of CO_3^{2-}, i.e. with O atoms pointing outwards of the surface for the first adsorbed layer and with O atoms pointing toward the surface for the second layer, this orientation can be justified considering that Li$^+$ cations are mainly placed between the CO_3^{2-} adsorbed layers and thus CO_3^{2-} adsorption is accompanied by efficient anion – cation coulombic interaction between the O atoms in CO_3^{2-} (negatively charged) and cations. The arrangements and ions orientation in the adsorbed layers around SWNTs should lead to charge accumulation as a function of distance to the nanotubes surface. Results in Figure S1 (Supporting Information) show charge peaks corresponding to cation and anion layers around the nanotubes, but the structure of the total charge density peaks is characterized by alternating positive and negative peaks, i.e. corresponding to an electrical double layer structuring.

The large densification of CO_3^{2-} ions around the SWNTs and the strength of CO_3^{2-} - SWNTs interactions reported in previous paragraphs should lead to remarkable differences between the dynamic properties of ions in the adsorbed layers and those in bulk liquid phases. These effects are quantified through the self-diffusion coefficients reported in Figure 5. CO_3^{2-} ions when adsorbed on the SWNTs outer

surface decrease their mobility in comparison with ions in the liquid phase (non-adsorbed). This effect is more pronounced in small diameter nanotubes and for ions in solvation layers closer to the nanotube surface. These results confirm that even ions in the third adsorbed layer, which are placed at 1.1 nm of the SWNTs, have low ionic mobility, as an effect of very efficient and strong CO_3^{2-} - SWNTs interactions. Regarding the effect of SWNT size on CO_3^{2-} mobility, lower diffusion rates for smaller nanotubes, considering that the SWNTs effect on CO_3^{2-} - SWNT interactions is linearly related to the number of the adsorption sites (i.e. C atoms into nanotubes), it can be rationalized by steric effects due to the larger extension of adsorbed layers in large nanotubes, which allows CO_3^{2-} mobility within the adsorbed layer.

Ions in Li$_2$CO$_3$ MAC can also be confined inside the SWNTs internal cavities by diffusion from the bulk liquid phases toward this region, which is spontaneously produced in MD simulations when SWNTs are placed in molten Li$_2$CO$_3$. The arrangement of confined ions is reported in Figure 6 for the studied SWNTs. As in the case of external adsorbed layers reported in previous sections, the behaviour of ions inside the SWNTs (cylindrical) cavities is characterized by a large orientation of CO_3^{2-} anions and in minor extension of Li$^+$ cations. In the case of narrow SWNT(6,6) (with 8.1 Å diameter) CO_3^{2-} anions are arranged in a single row following the central SWNT longitudinal axis, with Li$^+$ adopting a shell around them, Figure 6a. The increase of SWNTs diameter leads to more complex arrangements of confined CO_3^{2-} anions, following the same pattern as for the external solvation shells, i.e. concentric shells with the number being dependent on the diameter of the internal SWNT cavity, two layers for SWNT(15,15) (diameter 20.3 Å) and four layers for SWNT(25,25) (diameter 33.8 Å), Figures 6b to 6d. Regarding the arrangement of confined Li$^+$, layers are more poorly defined than for CO_3^{2-} (as for the case of external solvation shells), Figures 6b and 6c, but they tend to be placed between the CO_3^{2-} peaks, Figure 6d. Therefore, confined ions follow a similar pattern to external solvation shells, with ions reorganization being largely dependent on SWNTs internal diameter. This effect is confirmed by the orientation of CO_3^{2-} ions, which are also disrupted in their planarity when confined and follow analogous pattern as those in external solvation shells (Figures 4 and 7), thus showing analogous confinement and solvation mechanisms guided by CO_3^{2-} adsorption with intermediate cation layers for maintaining anion-

cation electrostatic interaction even upon confinement. Likewise, the number of confined anions and cations follows the 1 anion : 2 cations ratio for all the considered nanotubes, Table 1, thus maintaining Li_2CO_3 stoichiometry and electrical neutrality in confined salts and showing that the structuring developed upon confinement by CO_3^{2-} anions is accompanied by Coulombic interaction with the cations.

The effect of cation type on the properties of MACs + SWNTs is analysed by considering Na_2CO_3, K_2CO_3 and the $Li_{0.87}Na_{0.63}K_{0.50}CO_3$ eutectic (EU) mixture. Regarding the solvation of SWNTs, results in Figure 8 show a large effect of the type of considered cation, although adsorption is inferred for all the studied MACs (e.g. the three well-defined adsorption layers closer to the nanotubes surface), the layering of CO_3^{2-} anions is largely dependent on the type of cation, with adsorbed peaks intensity decreasing with increasing cation size (Li < Na < K). Likewise, the EU shows a behaviour intermediate between those for Li_2CO_3 and Na_2CO_3, thus confirming the role of cation size on the development of CO_3^{2-} guided adsorption layers. This can be justified considering the disrupting effect of large cations on the structuring of adsorbed layers by decreasing the number of adsorbed CO_3^{2-} anions, and thus decreasing the anion – SWNT interactions. The latter is quantified by the decreasing interaction energy with increasing cation size, as shown in Figure 1. The disrupting effect of larger cation size on the structuring of CO_3^{2-} adsorbed layers is confirmed by the results in Figures 9a to 9c, these distributions, when compared with the one in Figure 3c for Li_2CO_3, show the disappearing of the ordered concentric circular arrangements around the SWNT(25,25) for MACs with larger cations than Li^+. This disruptive effect is also confirmed by the CO_3^{2-} - CO_3^{2-} radial distribution functions, RDFs, for ions in the first solvation shell reported in Figure 9d. In the case of Li_2CO_3, consecutive peaks corresponding to the arrangement reported in Figure 3c are inferred, but as the cation size increases, the first RDF increases its distance (i.e. CO_3^{2-} anions are placed far from their neighbouring ones) and additional peaks have almost vanished. In the case of EU, the situation is intermediate, i.e. in between the observed behaviour for Li_2CO_3 and those for the other MACs. The behaviour of confined MACs follows the same pattern, CO_3^{2-} anions develop layering upon confinement for all the studied ions, but it is less remarkable for MACs with Na^+ or K^+ cations or EU (Figure S2, Supporting Information) system than in the case with Li^+ cations (Figure 6c). The disruptive effect on the confinement of MACs

with larger cations is confirmed by RDFs reported in Figure 10 showing an increase of ion-ion distances (both for anion-cation and anion-anion ones), which agrees with the number of confined ions reported in Table 1. Nevertheless, it should be remarked that the 1:2 anion-cation ratio is maintained for all the considered MACs, leading to electrical neutrality of confined MACs. Therefore, although the structure of confined MACs is guided by the trend of CO_3^{2-} anions to develop well-ordered layers following the SWNTs geometry, thus increasing anion-SWNTs interactions, the CO_3^{2-} confinement is accompanied by the penetration of the corresponding cations in stoichiometric amounts thus, limiting the number of confined CO_3^{2-} anions and decreasing the strength of ion-SWNTs interactions, Figure 1.

MACs + C60 fullerene

The second type of systems considered in this work were mixtures formed by C60 fullerenes and MACs. In an initial stage a single C60 fullerene was surrounded by MACs to mimic low concentration C60 solutions in MACs and to analyse the solvation behaviour of MACs. Results in Figure 11a show RDFs between the C60 center-of-mass and the corresponding ions in the studied MACs, i.e. the distribution of MACs in the solvation shells around the fullerene. In the case of Li_2CO_3, three well-defined solvation shells are inferred for CO_3^{2-} anions (spaced 3.5 Å, as in the case of shells around SWNTs, Figure 2), and Li^+ layers placed between CO_3^{2-} ones, with the first one above the first CO_3^{2-} one, i.e. CO_3^{2-} ions placed closer to the C60 surface. The comparison of results in Figures 2 and 11a shows similar solvation patterns around SWNTs and C60 fullerenes. The increase of cation size in MACs (Na^+ and K^+) leads to a shifting of the first CO_3^{2-} adsorbed layer and the vanishing of further solvation shells, Figure 11a. Likewise the arrangement of cations changes on going from Li^+ to Na^+ and K^+, with cations shifting toward the region occupied by CO_3^{2-} anions closer to the fullerene surface. In the case of EU system, the CO_3^{2-} solvation shells are mostly maintained in comparison with Li_2CO_3 although the peaks are slightly shifted from the fullerene surface. For EU, Na^+ and K^+ cations are placed in the same first CO_3^{2-} adsorbed shell whereas Li^+ cations are placed between the first and the second CO_3^{2-} solvation shells, thus showing that EU has an intermediate behaviour between that of pure MACs, and the distribution of cations seems to be independent of the considered MAC. The number of ions in the corresponding solvation shells, N, is reported in

Figures 11b and 11c. The number of adsorbed CO_3^{2-} anions decreases with increasing cation size in the MAC, with the EU showing an intermediate behaviour between Li_2CO_3 and the remaining MACs and analogously is inferred for the number of cations. Nevertheless, the number of anions and cations in each adsorbed layer follows the 1:2 anion:cation ratio confirming the electrical neutrality of the whole adsorbed layers and showing an analogous mechanism of adsorption with the SWNTs case. The distribution of ions in the first solvation shell around C60 fullerene is shown in Figure14. In the case of Li_2CO_3, Figure 12a, the Li^+ cation layer placed above the CO_3^{2-} layer and extending around the whole fullerene surface. In the case of MACs with Na^+ and K^+ cations the arrangement is completely different, Figures 12b and 12c, with both cations and CO_3^{2-} anions sharing the surface, in agreement with the RDFs reported in Figure 11a which showed the shifting of cations toward regions occupied by CO_3^{2-} ions in the first layer, thus leading to spots corresponding to cations and anions evenly distributed on the fullerene surface. In the case of EU mixture, Figure 12d, cations (including Li^+) and CO_3^{2-} anions are evenly distributed on the C60 surface, and in this case the presence of Na^+ and K^+ cations affects the Li^+ distribution, which is completely different to that for Li_2CO_3. The strength of ion-C60 interactions are quantified through intermolecular interaction energies reported in Figure 13, negative values are inferred for CO_3^{2-} - C60, with lower values than for CO_3^{2-} - SWNTs, Figure 1, because of the lower number of C atoms, but showing a very efficient solvation of C60 fullerene. Moreover, these energies decrease with increasing size of the involved cation, with EU showing an intermediate behaviour, Figure 13a, which agree with results in Figure 11. In the case of cation – C60 interaction energies, Figure 13b, small values are inferred for all the considered cations and MACs, with negative values for Li^+ and positive for Na^+ and K^+, but in all the cases the total ion-C60 energies (sum of cation and anion contributions) is large and negative confirming the efficient C60 solvation by the studied MACs although decreasing with increasing with cation size. The values of interaction energies for the EU show efficient solvation, which considering the low melting point, compared to other MACs, it can be used for C60 solution in required applications.

To study the effect of larger C60 concentrations on MACs properties a system composed by 6 C60 fullerenes in the considered simulation boxes were studied (Table S2, Supporting Information). The comparison between the properties of neat MAC (i.e.

in absence of C60) and the system containing the 6 C60 fullerenes are reported in Figure 14. The presence of this large concentration of C60 leads to remarkable changes in MACs structuring for all the considered systems. Regarding CO_3^{2-} - CO_3^{2-} interactions, RDFs reported in Figure 14a, show the disruptive effect of C60 on the anionic arrangement, decreasing the number of ions in the first solvation shell and almost vanishing CO_3^{2-} - CO_3^{2-} arrangement beyond the first solvation shell. In the case of CO_3^{2-} - cation interactions, Figure 14b, the long-range arrangement, especially for Li$_2$CO$_3$, is also weakened. Therefore, these results show that large C60 concentrations disrupt the anion-cation interactions in the considered MACs, which are weakened for solvating the available C60, because of the efficient CO_3^{2-} adsorption on the shells around the C60 fullerenes.

Conclusions

A theoretical study using molecular dynamics simulations on the properties of molten alkali carbonates with carbon nanotubes and fullerenes is reported in this work considering the effect of the involved cation, and the characteristics of the carbon nanomaterials. In the case of carbon nanotubes, the development of concentric adsorbed layers of CO_3^{2-} anions control the properties of the solvation shells around the nanotubes. The arrangement of CO_3^{2-} anions is almost planar regarding the nanotube surface with oxygen atoms deviating from the molecular plane to develop efficient Coulombic interaction with the corresponding cations placed above the anion adsorbed layers. Therefore, solvation shells are characterized by alternating negative – positive layers developing electrical double layer arrangement. Regarding the ions' confinement inside the nanotubes' cavities, configurations totally analogous to the one in the outer solvation shells are developed with the number of confined anions and cations following the stoichiometry of the carbonates. The adsorbed and confined CO_3^{2-} and cation layers are more ordered with increasing nanotube diameter and are more disordered, and thus less effective solvation, with increasing cation size. In the case of C60 fullerenes, solvation shells follow analogous pattern to those in carbon nanotubes, CO_3^{2-} being efficiently adsorbed on the fullerene surface with well-ordered layers being developed beyond the first solvation shell, especially for MACs with Li$^+$

cation. In the case of largely concentrated C60 solutions, the presence of fullerenes largely disrupts the anion-cation interactions for maintaining the solvation efficiency of fullerenes, which can be related to high solubility of these fullerenes in MACs. In all studied carbon nano-systems, the considered eutectic mixture, which has lower melting point compared to the primary MACs, show good solvation properties regarding nanotubes and fullerenes, and thus eutectic MAC + carbon nano-systems can be considered as suitable technological platforms for moderate temperature applications.

Acknowledgements

Supporting Information

Table S1 (MD force field parameterization for systems used along this work); Table S2 (description of systems used for MD simulations); Figure S1 (radial charge density profiles); Figure S2 (arrangements around C60.)

References

(1) González-Roubaud, E.; Pérez-Osorio, D.; Prieto, C. Review of Commercial Thermal Energy Storage in Concentrated Solar Power Plants: Steam vs. Molten Salts. *Renew. Sust. Ener. Rev.* **2017**, *80*, 133-148.

(2) Vignarooban, K.; Xu, X.; Arvay, A.; Hsu, K.; Kannan, A. M. Heat Transfer Fluids for Concentrating Solar Power Systems – A review. *Appl. Energ.* **2015**, *146*, 383-396.

(3) Nunes, V. M. B.; Queirós, C. S.; Lourenco, M. J. V.; Santos, F. J. V., Nieto de Castro, C. A. Molten Salts As Engineering Fluids – A Review: Part I. Molten alkali nitrates. *Appl. Energ.* **2016**, *183*, 603-611.

(4) Zhang, H. L.; Baeyens, J.; Degreve, J.; Caceres, G. Concentrated solar power plants: Review and Design Methodology. *Renew. Sust. Energ. Rev.* **2013**, *22*, 466-481.

(5) Parrado, C.; Marzo, A.; Fuentealba, E.; Fernández, A. G. 2050 LCOE Improvement Using New Molten Salts for Thermal Energy Storage in CSP Plants. *Renew. Sus. Energ. Rev.* **2016**, *57*, 505-514.

(6) Vignarooban, K.; Xu, X.; Hsu, K.; Kannan, A. M. Heat Transfer Fluids for Concentrating Solar Power Systems – A Review. *Appl. Energ.* **2015**, *146*, 383-396.

(7) Madathil, P. K.; Balagi, N.; Saha, P.; Bharali, J.; Rao, P. V. C.; Choudary, N. V.; Ramesh, K. Preparation and Characterization of Molten Salt Based Nanothermic Fluids with Enhanced Thermal Properties for Solar Thermal Applications. *Appl. Therm. Eng.* **2016**, *109*, 901-905.

(8) Serrano-López, R.; Fradera, J.; Cuesta-López, S. Molten Salts Database for Energy Applications. *Chem. Eng. Process.* **2013**, *73*, 87-102.

(9) Wang, T.; Mantha, D.; Reddy, R. G. Thermal Stability of the Eutectic Composition in $LiNO_3$–$NaNO_3$–KNO_3 Ternary System Used for Thermal Energy Storage. *Solar Energ. Mat. Sol. C.* **2012**, *100*, 162-168.

(10) Peng, Q.; Wei, X.; Dinag, J.; Yang, X.; Yang, X. High-Temperature Thermal Stability of Molten Salt Materials. Int. J. Energy Res. 2008, 32, 1164-1174.

(11) Vignarooban, K.; Xu, X.; Arvay, Hsu, A.; Kannan, A, M. Heat Transfer Fluids for Concentrating Solar Power Systems – A Review. *Appl. Energ.* **2015**, *146*, 383-396.

(12) Mohn, H.; Wendt, H. Molecular Thermodynamics of Molten Salt Evaporation. Z. Phys. Chem. **1995**, *192*, 101-119.

(13) An, X.; Chen, J.; Zhang, P.; Tang, Z.; Wang, J. Determination and Evaluation of the Thermophysical Properties of an Alkali Carbonate Eutectic Molten Salt. *Faraday Discuss.* **2016**, *190*, 327-338.

(14) Gheribi, A. E.; Torres, J. A.; Chartrand, P. Recommended values for the thermal conductivity of molten salts between the melting and boiling points. *Solar Energ. Mat. Sol. C.* **2014**, *126*, 11-25.

(15) Zhao, Q. G.; Hu, C. X.; Liu, S. J.; Guo, H.; Wu, Y. T. The Thermal Conductivity of Molten NaNO3, KNO3 and Their Mixtures. *Energy Procedia* **2017**, *143*, 774-779.

(16) Frangini, S.; Masi, A. Molten Carbonates for Advanced and Sustainable Energy Applications: Part II. Review of Recent Literature. *Int. J. Hydrogen Energ.* **2016**, *41*, 18971-18994.

(17) Fernandes, D.; Pitie, F.; Cáceres, F.; Baeyens, J. Thermal Energy Storage: "How Previous Findings Determine Current Research Priorities". *Energy* **2012**, *39*, 246-257.

(18) Chieruzzi, M.; Cerritelli, G. F.; Miliozzi, A.; Kenny, J. M. Effect of Nanoparticles on Heat Capacity of Nanofluids Based on Molten Salts as PCM for Thermal Energy Storage. *Nanoscale Res. Lett*. **2013**, *8*, 448.

(19) Awad, A.; Navarro, H.; Ding, Y.; Wen, D. Thermal-Physical Properties of Nanoparticle-Seeded Nitrate Molten Salts. *Renew. Energ.* **2018**, 120, 275-288.

(20) Manfred, B. Molten Carbonate Fuel cells: A High Temperature Fuel Cell on the Edge to Commercialization. *J. Power Sources* **2006**, *160*, 842.

(21) Dicks, A. L. Molten Carbonate Fuel Cells. *Curr. Opin. Solid St. M.* **2004**, *8*, 379-383.

(22) Mcphail, S.J.; Leto, L.; Della Pietra, M.; Cigolotti, V.; Moreno, A. International status of molten carbonate fuel cells. **2015**.

(23) Hsieh, P.H.; Robert Selman, J.; McPhail, S.J.; Molten carbonate fuel cells. In: Fuel cells in the waste-to-energy chain, vol. 45. London: Springer; **2012.**

(24) Chery, D.; Lair, V.; Cassir, M.; Overview on CO2 Valorization: Challenge of Molten Carbonates. *Front. Energy Res.* **2015**, *3*, 43.

(25) Wee, J. H. Carbon Dioxide Emission Reduction Using Molten Carbonate Fuel Cell Systems. *Renew. Sust. Energ*. *Rev.* **2014**, *32*, 178-191.

(26) Forsyth, J.; Lodge, S.; Consonni, S.; Di Bona, D.; Gatti, M.; Martelli, E.; Scaccabarozzi, R.; Vigano, F. Evaluation of Five Alternative CO2 Capture Technologies with Insights to Inform Further Development. *Energy Procedia* **2017**, *114*, 2599-2610.

(27) Olsen, E.; Tomkute, V. Carbon Capture in Molten Salts. *Energy Sci. Eng*. **2013**, *1*, 144-150.

(28) Deng, B.; Tang, J.; Mao, X.; Song, Y.; Zhu, H.; Xiao, W.; Wang, D. Kinetic and Thermodynamic Characterization of Enhanced Carbon Dioxide Absorption Process with Lithium Oxide-Containing Ternary Molten Carbonate. *Environ. Sci. Technol.* **2016**, *50*, 10588-10595.

(29) Patricio, S. G.; Papaioannou, E. I.; Ray, B. M.; Metcalfe, I. S.; Marques, F. M. B. Composite CO2 Separation Membranes: Insights on Kinetics and Stability. *J. Membrane Sci.* **2017**, *541*, 253-261.

(30) Näfe, H. Composite CO2 Separation Membranes: Insights on Kinetics and Stability. *ECS Solid State Sci. Technol.* **2014**, *3*, N23-N29.

(31) Yang, Z.; Zhu, Y.; Han, M. Synthesis and Characterization of Gadolinium Doped Ceria-Carbonate Dual-Phase Membranes for Carbon Dioxide Separation. *J. Alloy Comp.* **2017**, *723*, 70-74.

(32) Gutiérrez, A.; Garroni, S.; Souentie, S.; Cuesta-López, S.; Yakoumis, I.; Aparicio, S. A Theoretical Study on Molten Alkali Carbonate Interfaces. *Langmuir* **2018**, OI: 10.1021/acs.langmuir.8b02907.

(33) Khanafer, K.; Tavakkoli, F.; Vafai, K.; AlAmiri, A. A Critical Investigation of the Anomalous Behavior of Molten Salt-Based Nanofluids. *Int. Commun. Heat Mass Trans*. **2015**, *69*, 51-58.

(34) Ueki, Y.; Fujita, N.; Kawai, M.; Shibahara, M. Molten Salt Thermal Conductivity Enhancement by Mixing Nanoparticles. *Fusion Eng. Des*. **2018**, DOI: https://doi.org/10.1016/j.fusengdes.2018.04.121

(35) Jo, B.; Benerjee, D. Enhanced Specific Heat Capacity of Molten Salt-Based Carbon Nanotubes Nanomaterials. *J. Heat Transfer* **2015**, *137*, 091013.

(36) Fatemi, S. M.; Foroutan, M. Recent Findings About Ionic Liquids Mixtures Obtained by Molecular Dynamics Simulation. *J. Nanostruct. Chem*. **2015**, *5*, 243-253.

(37) Ghoufi, A.; Szymczyk, A.; Malfrey, P. Ultrafast diffusion of Ionic Liquids Confined in Carbon Nanotubes. *Scientific Reports* **2016**, *6*, 28518.

(38) Roest, D. L.; Ballone, P.; Bedeaux, D.; Kjelstrup, S. Molecular Dynamics Simulations of Metal/Molten Alkali Carbonate Interfaces. *J. Phys. Chem. C*. **2017**, *121*, 17827-17847.

(39) Chen, C.; Tran, T.; Olivares, R.; Wright, S.; Sun, S. Coupled Experimental Study and Thermodynamic Modelling And Thermal Stabilty of $L2CO3 - Na2CO3 - K2CO3$ Based Salts. *J. Solar Energ. T. ASME* **2014**, *136*, 031017.

(40) Lyubartsev, A. P.; Laaksonen, A. MDynaMix - A Scalable Portable Parallel MD Simulation Package for Arbitrary Molecular Mixtures. *Comput. Phys. Commun*. **2000**, *128*, 565-589.

(41) Aparicio, S.; Atilhan, M. Molecular Dynamics Study of Carbon Nanostructures in N-Methylpiperazinium Lactate Ionic Liquid. *J. Phys. Chem. C* **2013**, *117*, 22046–22059.

(42) Martínez, L.; Andrade, R.; Birgin, E. G.; Martínez, J. M. Packmol: A Package for Building Initial Configurations for Molecular Dynamics Simulations. *J. Comput. Chem.* **2009**, *30*, 2157-2164.

(43) Thostenson, E.; Li, C.; Chou, T. Nanocomposites in context. *Composites Science and Technology*. **2005**, *65*, 3–4.

(44) Eletskii, A. V.; Smirnov, B. M. Fullerenes. (Vol 163, pg 47, 1993) *Usp. Fiz. Nauk*. **1993**, *163* (2), 33.

(45) Milliken, J.; Keller, T. M.; Baronavski, A. P.; McElvany, S. W.; Callahan, J. H.; Nelson, H. H. Thermal and oxidative analyses of buckminsterfullerene, C60. *Chemistry of Materials*. **1991**, *3*(3), 386-387.

(46) Churilov, G.N. Plasma synthesis of fullerenes. *Instruments and experimental techniques*. **2000**, *43* (1), 1-10.

(47) Kolodney, E.; Tsipinyuk, B.; Budrevich, A. The thermal stability and fragmentation of C60 molecule up to 2000 K on the milliseconds time scale. *J. Chem. Phys*. **1994**, *100*, 8542.

(48) Tuckerman, M.; Berne, B. J.; Martyna, G. J. Reversible Multiple Time Scale Molecular Dynamics. *J. Chem. Phys*. **1992**, *97*, 1990-2001.

Table 1. Number of ions, *N*, confined inside SWNT(25,25) for the reported (Li$_2$CO$_3$ or Na$_2$CO$_3$ or K$_2$CO$_3$ or Li$_{0.87}$Na$_{0.63}$K$_{0.50}$CO$_3$, EU) + SWNT(25,25) systems.

salt	N_{CO3}	N_{cation}	$N_{cation(s)}$ / N_{CO3}
Li$_2$CO$_3$	375±3	754±5	2.0
Na$_2$CO$_3$	251±3	504±5	2.0
K$_2$CO$_3$	154±3	308±5	2.0
Li$_{0.87}$Na$_{0.63}$K$_{0.50}$CO$_3$	266±2	248±2 (Li)	2.0
		157±2 (Na)	
		131±1 (K)	

Figure Captions

Figure 1. Intermolecular interaction energies (sum of Lennard-Jones and coulombic contributions, E_{inter}) for ion – SWNT interactions in (Li$_2$CO$_3$ or Na$_2$CO$_3$ or K$_2$CO$_3$ or Li$_{0.87}$Na$_{0.63}$K$_{0.50}$CO$_3$ (eutectic mixture, EU)) + SWNT ((6,6) or (15,15) or (25,25)) at 1023 K (Li$_2$CO$_3$), 1153 K (Na$_2$CO$_3$), 1193 K (K$_2$CO$_3$) and 673 K (Li$_{0.87}$Na$_{0.63}$K$_{0.50}$CO$_3$) and 1 bar. Results in panel e correspond to the sum of cation – SWNT + anion – SWNT contributions for each system.

Figure 2. Snapshots of CO_3^{2-} ions around SWNTs and the corresponding radial number density profiles of CO_3^{2-} and Li$^+$ ions (center-of-mass), with r being the distance to the radial axis of the SWNTs and r_{wall} the position of the SWNTs carbon atoms for Li$_2$CO$_3$ + SWNT systems. A extended plot of the solvation shells around SWNT(25,25) is showed at the top of the figure (blue arrow) showing the three first solvation shells.

Figure 3. (a to c) Snapshots of the arrangement of C atoms in CO_3^{2-} ions on top of SWNTs, for the first solvation shells, and (d) the corresponding longitudinal number density profiles of CO_3^{2-} (blue) and Li$^+$ (red) ions (center-of-mass), with R being the distance along the radial axis of the SWNTs. Vertical dashed lines show the position of the SWNTs carbon atoms for Li$_2$CO$_3$ + SWNT systems. Filled symbols show the position of maxima for the sake of visibility. White arrow indicates atoms wrapping around SWNT surface.

Figure 4. Radial number density profiles of CO_3^{2-} ions (C and O1, O2, O3 atoms), with r being the distance to the radial axis of the SWNT and r_{wall} the position of the SWNT carbon atoms for Li$_2$CO$_3$ + SWNT(25,25) system. The snapshot is showed to clarify the orientation of CO_3^{2-} ions regarding SWNT surface

Figure 5. Ratio of CO_3^{2-} self-diffusion coefficients in i solvation shell to bulk liquid phase, D_{shell}/D_{bulk} (for first, second and third solvation shells as showed in snapshot), for Li$_2$CO$_3$ + SWNTs systems. D_{bulk} (Li$^+$)= 4.5×10^{-5} m^2 s^{-1} and D_{bulk} (CO_3^{2-})= 0.52×10^{-5} m^2 s^{-1}.

Figure 6. (a to c) Snapshots and (d) radial number density profiles of CO_3^{2-} and Li$^+$ ions (center-of-mass), with r being the distance to the radial axis of the SWNTs. Vertical dashed lines show the position of the SWNTs carbon atoms for Li$_2$CO$_3$ + SWNT systems. Points indicate the position of the maxima for guiding purposes.

Figure 7. Radial number density profiles of CO_3^{2-} ions (C and O1, O2, O3 atoms), with r being the distance to the radial axis of the SWNT for Li$_2$CO$_3$ + SWNT(25,25) system.

Figure 8. Radial number density profiles of CO_3^{2-} (center-of-mass), with *r* being the distance to the radial axis of the SWNTs and r_{wall} the position of the SWNT carbon atoms for (Li$_2$CO$_3$ or Na$_2$CO$_3$ or K$_2$CO$_3$ or Li$_{0.87}$Na$_{0.63}$K$_{0.50}$CO$_3$, EU) + SWNT(25,25) systems.

Figure 9. (a to c) Snapshots of CO_3^{2-} (center-of-mass), for (Li$_2$CO$_3$ or Na$_2$CO$_3$ or K$_2$CO$_3$ or Li$_{0.87}$Na$_{0.63}$K$_{0.50}$CO$_3$, EU), in the first external solvation shell around SWNT(25,25) system and (d) CO_3^{2-} - CO_3^{2-} center-of-mass radials distribution functions, *g*(*r*), in the same shell. Numbers inside (d) panel indicate the position of the first maxima.

Figure 10. Center-of-mass radials distribution functions, *g*(*r*), for the reported ions confined inside SWNT(25,25) for Li$_2$CO$_3$ or Na$_2$CO$_3$ or K$_2$CO$_3$ or Li$_{0.87}$Na$_{0.63}$K$_{0.50}$CO$_3$, EU. Numbers inside each panel indicate the position of the maxima.

Figure 11. (a) Radial distribution functions, *g*(*r*), between the fullerene C60 and the center-of-mass of ions and (b,c) the corresponding solvation numbers, *N*, for Li$_2$CO$_3$ or Na$_2$CO$_3$ or K$_2$CO$_3$ or Li$_{0.87}$Na$_{0.63}$K$_{0.50}$CO$_3$, EU, + fullerene C60. Numbers inside each panel indicate the position of the maxima.

Figure 12. Ions distribution in the first solvation shell around fullerene C60 for Li$_2$CO$_3$ or Na$_2$CO$_3$ or K$_2$CO$_3$ or Li$_{0.87}$Na$_{0.63}$K$_{0.50}$CO$_3$, EU, + fullerene C60.

Figure 13. Intermolecular interaction energies (sum of Lennard-Jones and coulombic contributions, E_{inter}) for ion – fullerene C60 interactions in (Li$_2$CO$_3$ or Na$_2$CO$_3$ or K$_2$CO$_3$ or Li$_{0.87}$Na$_{0.63}$K$_{0.50}$CO$_3$ (eutectic mixture, EU)) + fullerene C60. Results in panel c correspond to the sum of cation − C60 + anion − C60 contributions for each system.

Figure 14. Radial distribution functions (center-of-mass), *g*(*r*), for the reported pairs in neat Li$_2$CO$_3$ or Li$_{0.87}$Na$_{0.63}$K$_{0.50}$CO$_3$, EU, and Li$_2$CO$_3$ or EU + fullerene C60.
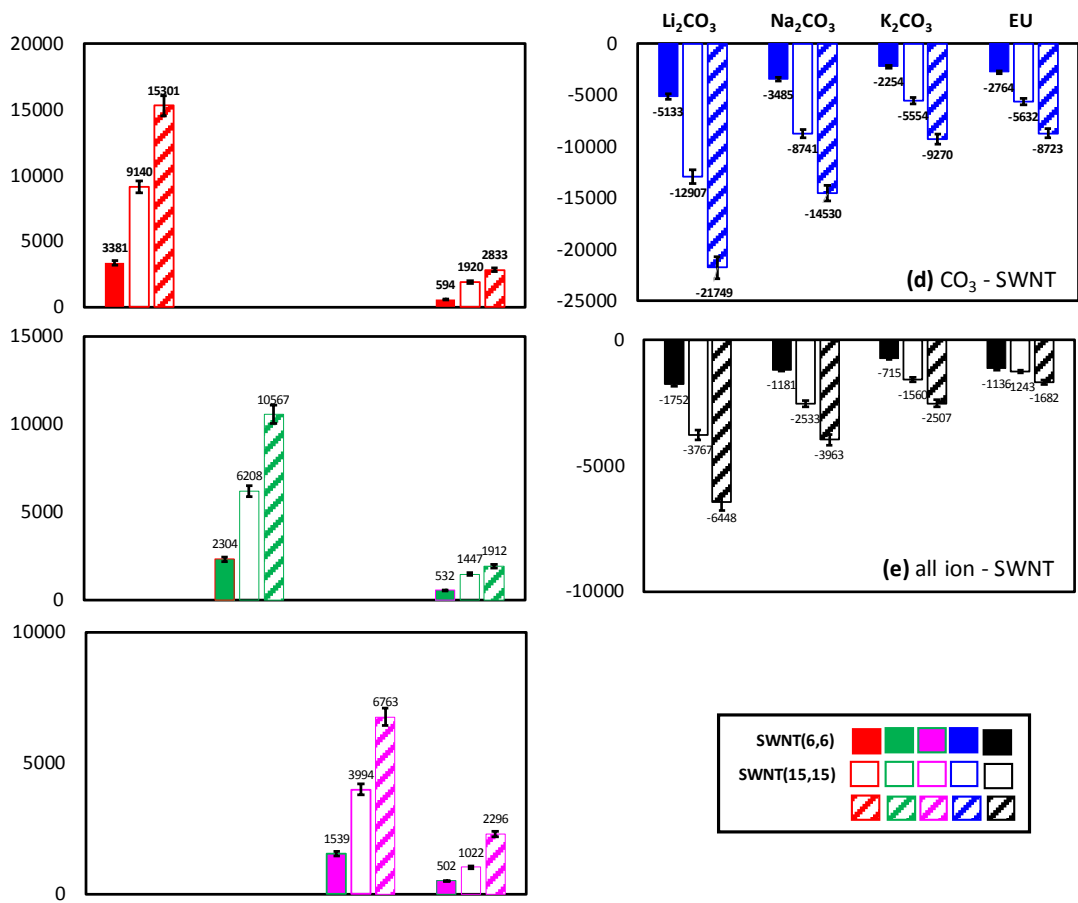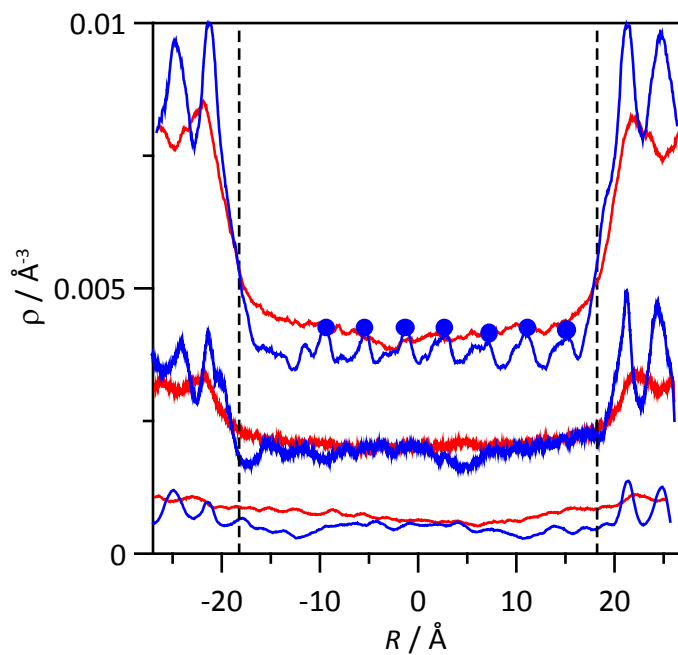
Figure 1.
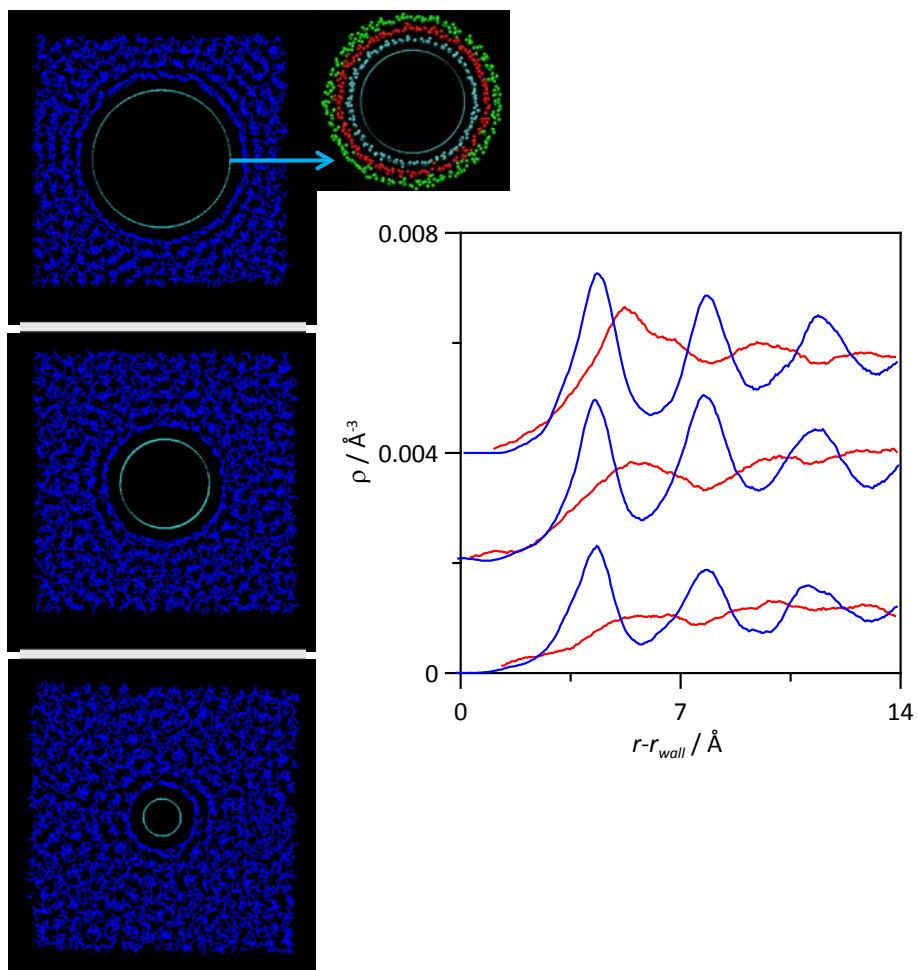
Figure 2.

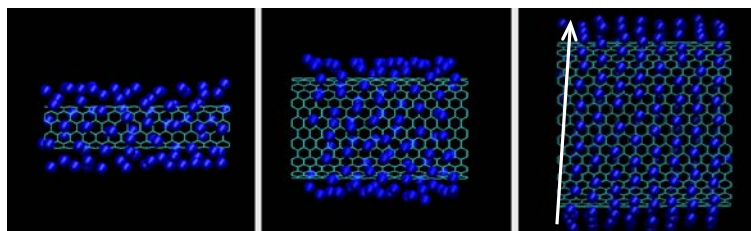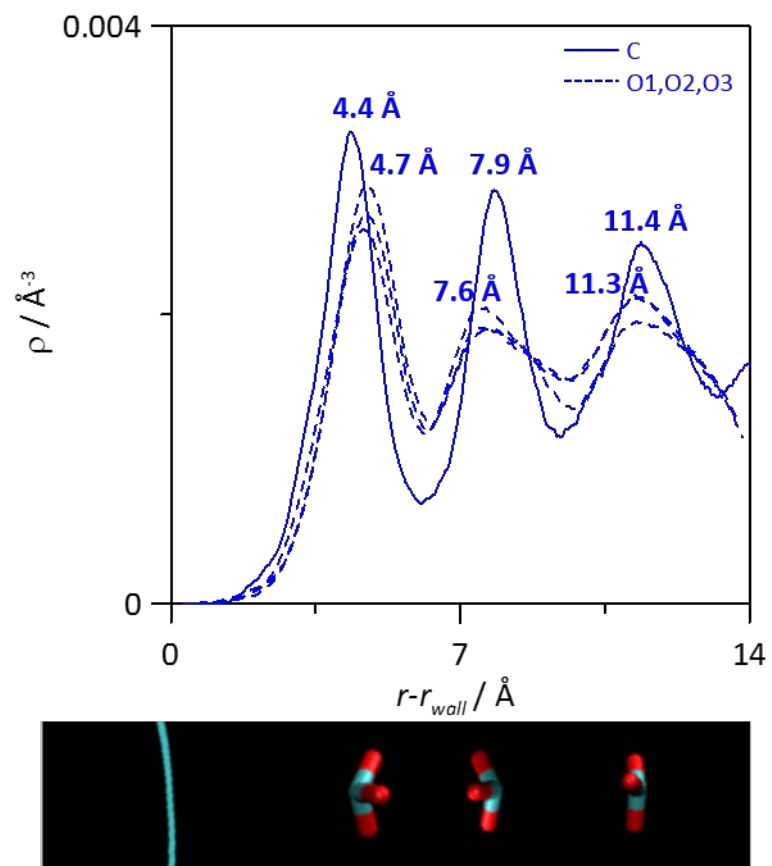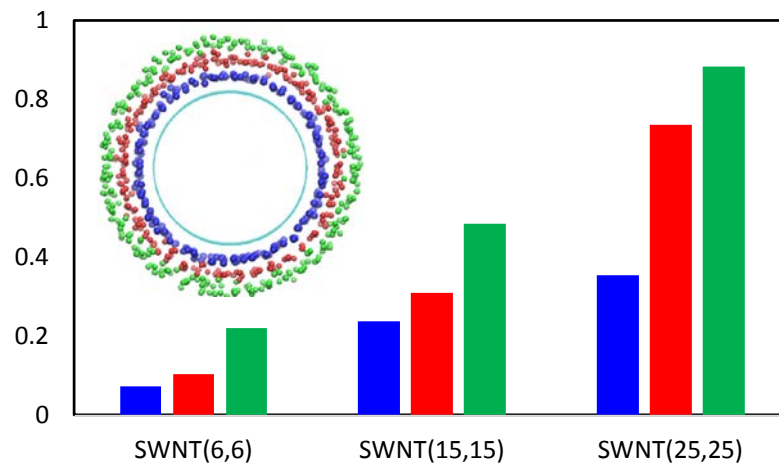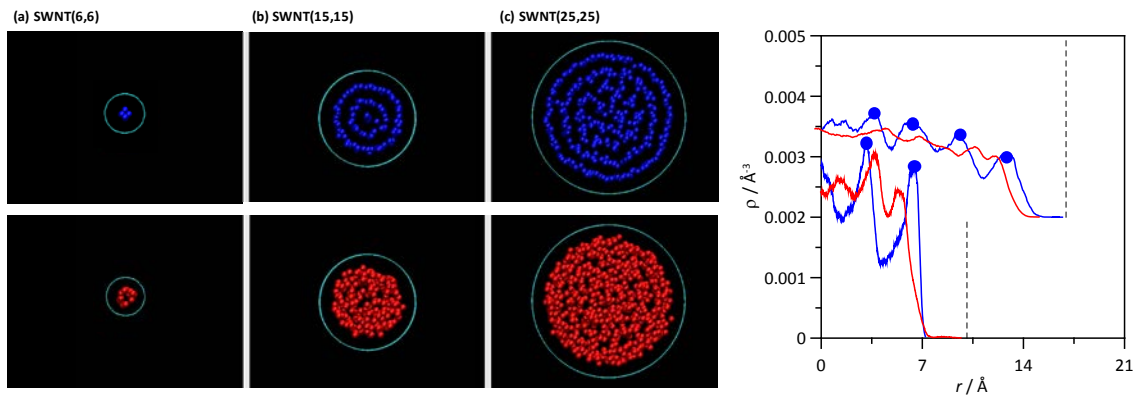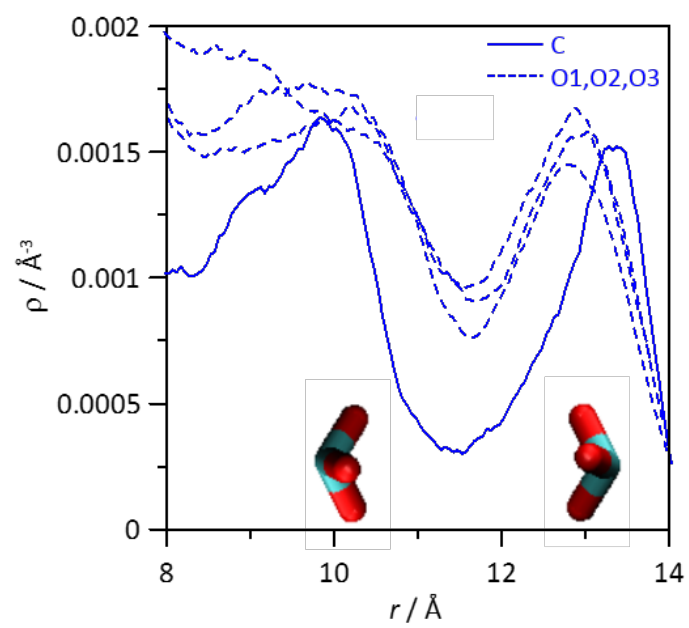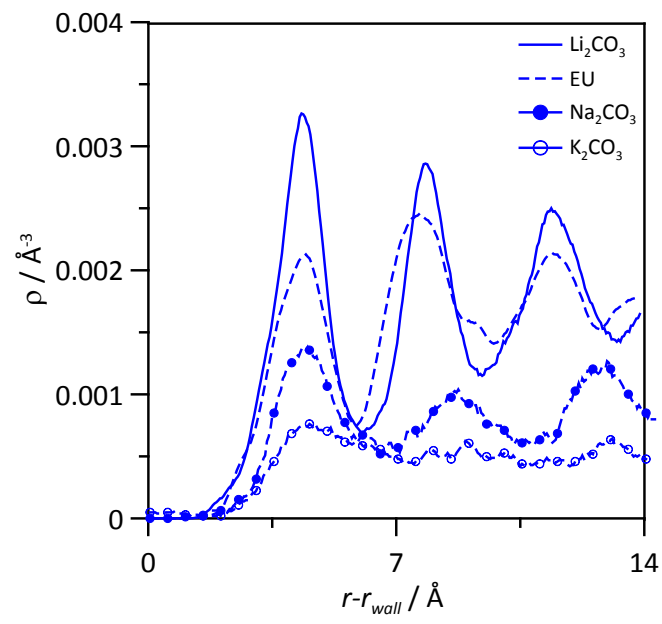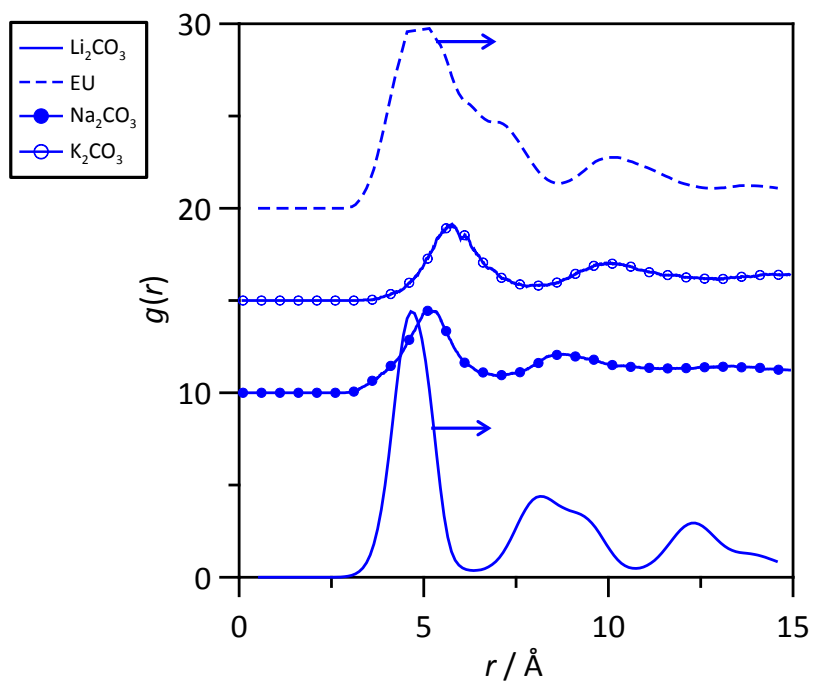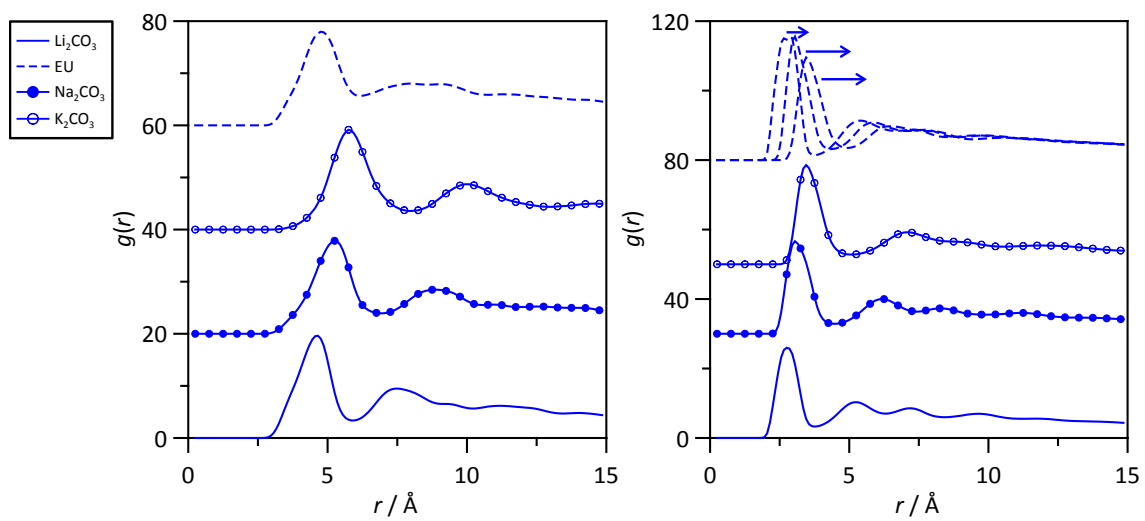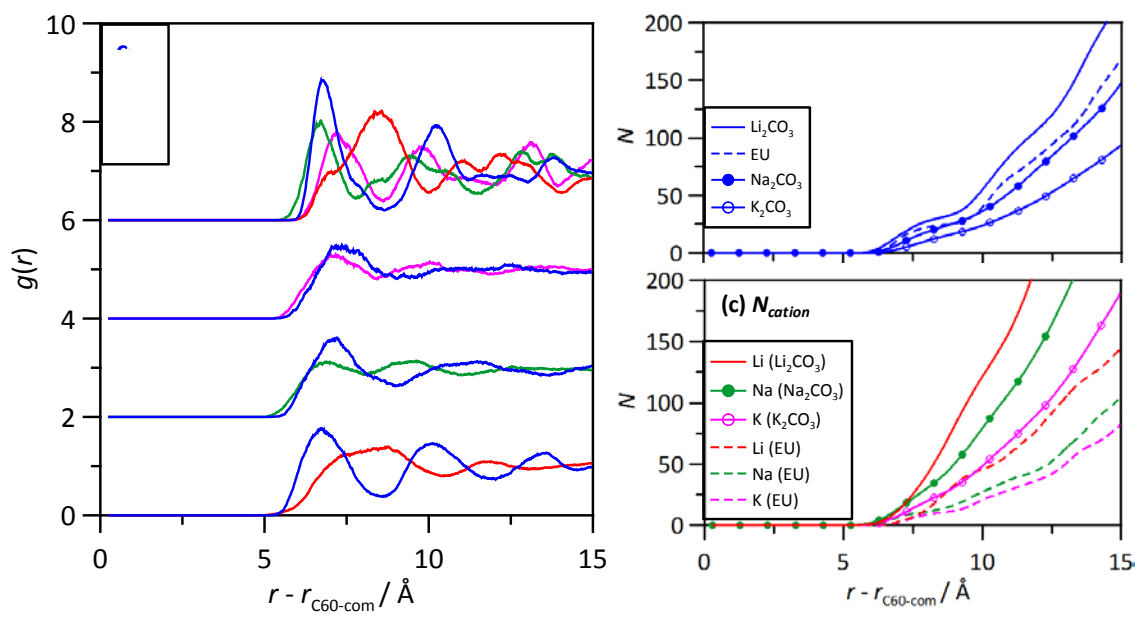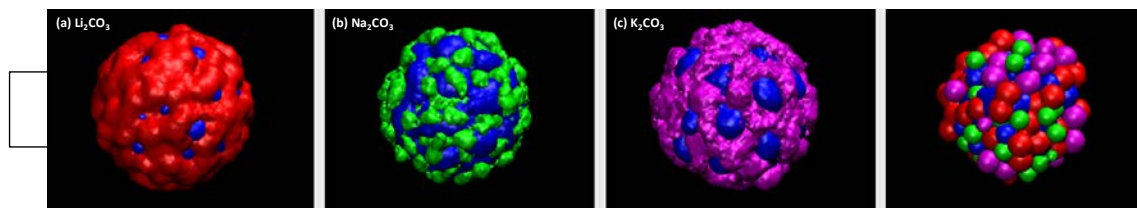Figure 3.

Figure 4.

Figure 5.

(a) SWNT(6,6)   **(b) SWNT(15,15)**   **(c) SWNT(25,25)**

Figure 6.

Figure 7.

Figure 8.
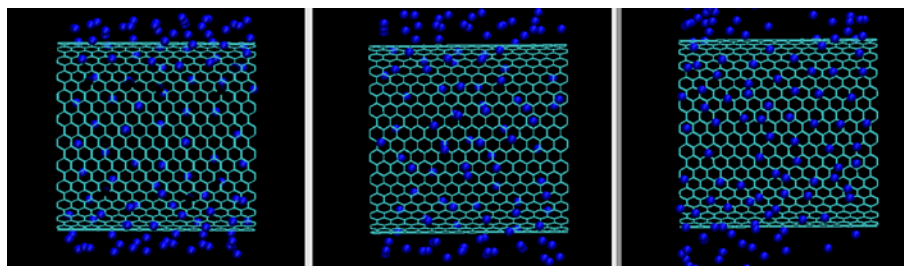
Figure 9.

Figure 10.

Figure 11.

(a) Li$_2$CO$_3$ (b) Na$_2$CO$_3$ (c) K$_2$CO$_3$

Figure 12.

Figure 13.

Figure 14.